Structure–Mechanical Stability Relations of Metal-Organic Frameworks via Machine Learning

Peyman Z. Moghadam[a,*,#], Sven M. J. Rogge[c,#], Aurelia Li[b], Chun-Man Chow[b], Jelle Wieme[c], Noushin Moharrami[d], Marta Aragones-Anglada[b], Gareth Conduit[e], Diego A. Gomez-Gualdron[f], Veronique Van Speybroeck[c], and David Fairen-Jimenez[b,*,‡]

[a]Department of Chemical and Biological Engineering, University of Sheffield, Mappin Street, Sheffield S1 3JD, UK

[b]Adsorption & Advanced Materials Laboratory (AAML), Department of Chemical Engineering & Biotechnology, University of Cambridge, Philippa Fawcett Drive, Cambridge CB3 0AS, UK

[c]Center for Molecular Modeling (CMM), Ghent University, Technologiepark 903, 9052 Zwijnaarde, Belgium

[d]TWI Ltd, Granta Park Great Abington, Cambridge, CB21 6AL, UK

[e]Cavendish Laboratory, University of Cambridge, J.J. Thomson Avenue, Cambridge CB3 0HE, UK

[f]Department of Chemical and Biological Engineering, Colorado School of Mines, Golden, Colorado 80401, United States

*e-mails: P. Z. M., p.moghadam@sheffield.ac.uk; D. F.-J., df334@cam.ac.uk

#Equal contributions

‡Lead contact

SUMMARY

The building block approach in the synthesis of metal-organic frameworks (MOFs) brings about a broad range of topologies and pore sizes that has fueled their immense exploration for energy-related applications. The necessity to design more stable structures is receiving growing recognition from the MOF community, where, besides thermal and chemical stability, MOFs' mechanical stability is critical to bring these materials to any reasonable energy application. Herein, we derive the first interactive map of the structure-mechanical landscape of MOFs by performing a multi-level computational analysis. First, we used high-throughput molecular simulations for 3,385 MOFs containing 41 distinct network topologies. Second, we developed a freely available machine learning algorithm to automatically predict the mechanical properties of existing and yet-to-be-synthesized MOFs. For distinct regions of the high-throughput space, in-depth analysis based on operando molecular dynamics simulations reveals the loss-of-crystallinity pressure within a given topology. The overarching mechanical screening approach presented here reveals the sensitivity on structural parameters such as topology, coordination characteristics, and the nature of the building blocks, and paves the way for computational as well as experimental researchers to assess and design MOFs with enhanced mechanical stability to accelerate the translation of MOFs to industrial applications.

INTRODUCTION

With ca. 88,000 structures present in the Cambridge Structural Database (CSD),(Moghadam et al., 2017b) metal-organic frameworks (MOFs) continue to amaze scientists due to their exceptional properties. MOFs are a unique class of porous coordination polymers synthesized in a self-assembly process from metal building units bridged by organic ligands. Because of their building block nature, MOFs allow for conscious design protocols, where structural properties such as topology, pore size and shape, as well as surface chemistry are tuneable.(Furukawa et al., 2013; Horike et al., 2009; Maurin et al., 2017; Zhou and Kitagawa, 2014) Such flexibility of design permits MOFs to find applications in a multitude of industrial settings such as gas storage(Mason et al., 2015; Thornton et al., 2017; Tian et al., 2018) and separation,(Bobbitt et al., 2017; Li et al., 2009; Moghadam et al., 2017a) catalysis(Rogge et al., 2017) and in the healthcare domain.(Faust, 2015; Horcajada et al., 2010; Miller et al., 2016; Teplensky et al., 2017)

Despite the versatility of MOFs, there are still fundamental issues preventing the large-scale industrial adoption of these materials. A large number of MOFs are prone to degradation and loss of crystallinity due to chemical reactions or the application of mechanical stress – an feature that is critical for the applicability of these material in industry.(Howarth et al., 2016; Tan and Cheetham, 2011; Tan et al., 2012) In particular, the mechanical stability of MOFs becomes crucial during the densification and pelletization process, where MOF powders are transformed into larger, shaped pellets.(Rubio-Martinez et al., 2017) A low mechanical stability manifests itself as partial pore collapse, unwanted phase transformations or even amorphization, often resulting in a reduction of adsorption capacity – a property central to the applicability of porous MOFs.(Peterson et al., 2013) Thus, making stable MOFs with open frameworks that allow for the diffusion of gases in and out of the pores is crucial to enable the large deployment of these materials for energy applications such as high pressure gas storage, fuel cell design and hydrocarbon separation processes.(Wang et al., 2017; Xiao and Xie, 2017; Zhang et al., 2017)

Dedicated studies on selected materials have helped to understand how mechanical stability and structural characteristics are intercorrelated.(Burtch et al., 2018; Coudert and Fuchs, 2016; Hajek et al., 2018; Kapustin et al., 2017; Moosavi et al., 2018; Ortiz et al., 2012; Rogge et al., 2018; Sarkisov et al., 2014; Vanduyfhuys et al., 2018a; Wu et al., 2013) However, so far, an overarching view on the influence of geometric properties, such as the topology, length of the building blocks and coordination characteristics, on the mechanical stability of MOFs is not available. To derive such general structure-mechanical stability

relationships for a diverse set of MOFs, a much higher number of materials needs to be screened in a systematic way and proper automatic analysis tools need to be adopted to obtain insight into the structural-mechanical stability space.

With the unparalleled potential to investigate thousands of structures in a short time, computational high-throughput screening (HTS)(Moghadam et al., 2016) is extremely well-suited to unravel trends in key MOF properties, establish structure-property relationships and guide future synthetic efforts. In the last years, HTS of MOFs has focused mostly on the characterization of geometric (e.g. pore size distribution, pore volume, surface area) and gas adsorption properties.(Bernini et al., 2014; Colón et al., 2014; Moghadam et al., 2016; Simon et al., 2015; Wilmer et al., 2012) Although this approach has delivered important insights, it has not yet been applied to MOFs' mechanical properties. One of the main remaining hurdles to achieve a meaningful exploration of the structure-stability landscape is the proper characterization of the underlying structural topology of the MOFs, which is expected to play a key role in the mechanical stability.(Sarkisov et al., 2014) Furthermore, certain topologies may impose limits for achievable structural features.

Having this idea present, the first question one needs to ask is which MOF database should be used to screen mechanical properties. In an outstanding contribution, Wilmer *et al.*(Wilmer et al., 2012) used a bottom-up approach to generate 137,000 materials by connecting a number of organic ligands and metal clusters (building blocks) used in MOFs. However, with this approach, only six topologies were created, and one single topology (i.e. primitive cubic unit, *pcu*) dominated over 90% of the database.(Sikora et al., 2014) Clearly, a much wider topological diversity can be found in the current ca. 88,000 MOFs present in the CSD.(Moghadam et al., 2017b) However, computer "on-the-fly" analysis of the underlying topologies for this many materials is far from trivial, as current topological analysis software such as TOPOS(Alexandrov et al., 2011) requires significant user involvement for each material analyzed. To tackle this issue and to target a topologically diverse representation of MOFs, Gomez-Gualdron and co-workers(Gómez-Gualdrón et al., 2016) used an automated reversed topological approach to construct a database of 13,512 MOFs by connecting a finite set of MOF building blocks into 41 predefined network topologies.

In the present work, we used part of this database of MOFs with known topologies to calculate the mechanical properties of a wide range of structures. By starting from such a diverse set of materials, we unveiled causal relationships between the mechanical robustness of MOFs in equilibrium, as expressed by the bulk and shear moduli, on the one hand, and the chemical-structural properties (e.g. type and coordination of the nodes, pore

size and shape), and, most importantly, topology, on the other hand. To further explore the potential of MOFs to be used under *operando* conditions, more advanced *ab initio*-based force field molecular dynamics calculations are performed to determine the effect of temperature on the mechanical robustness and the critical pressure a material can withstand before crystallinity is lost.(Rogge et al., 2015; Rogge et al., 2016b) This thorough study is backed-up by a web-domain visualization tool that enables users to interactively probe the structure-mechanical stability landscape of MOFs along 5 dimensions. Furthermore, artificial neural networks are introduced here as a powerful machine-learning algorithm not only to predict the mechanical properties of existing and yet-to-be-synthesized MOFs, but also to elucidate the sensitivity of the obtained mechanical stability window on the topology. To the best of our knowledge, this is the first high-throughput screening of mechanical properties in MOFs, providing not only in-depth insights on structure-mechanical stability relationships, but also enabling the rational selection and design of MOFs with better mechanical properties. This is key to bring the application of MOFs for industrial applications in the energy field and beyond closer to reality.

RESULTS AND DISCUSSION

Selection of MOFs with diverse topologies. Starting from the 13,512 MOFs generated by Gomez-Gualdron *et al.,*(Gómez-Gualdrón et al., 2016) we selected those MOFs that are composed of the organic ligands and nodes depicted in Figure 1, resulting in a shortlist of 3,385 MOFs. In Figure 1, the entire list of the 14 organic ligands and 28 organic or metal-based nodes we used in this study are shown; the selected ligands are classified according to their length, while the nodes are classified according to their coordination number (i.e. the number of organic ligand connections for every metal-based or organic node). From the original database, we deliberately selected non-functionalized linkers in a manner as to reflect the effect of linker length with one, two and three additional carbon-carbon triple bonds (T), phenyl linker chemistry: from simple acetylenedicarboxylic acid and benzene-1,4-dicarboxylic acid, rings (P), or nitrogenated phenyl rings (N, tetrazines). All structures are made up of perfect crystals, i.e., no defects or residual solvent are present. The database used here contains 41 distinct topologies creating a widely diverse set of geometrical properties which enables a thorough exploration of the structure-mechanical stability relations in MOF space (Figs. S1-2).
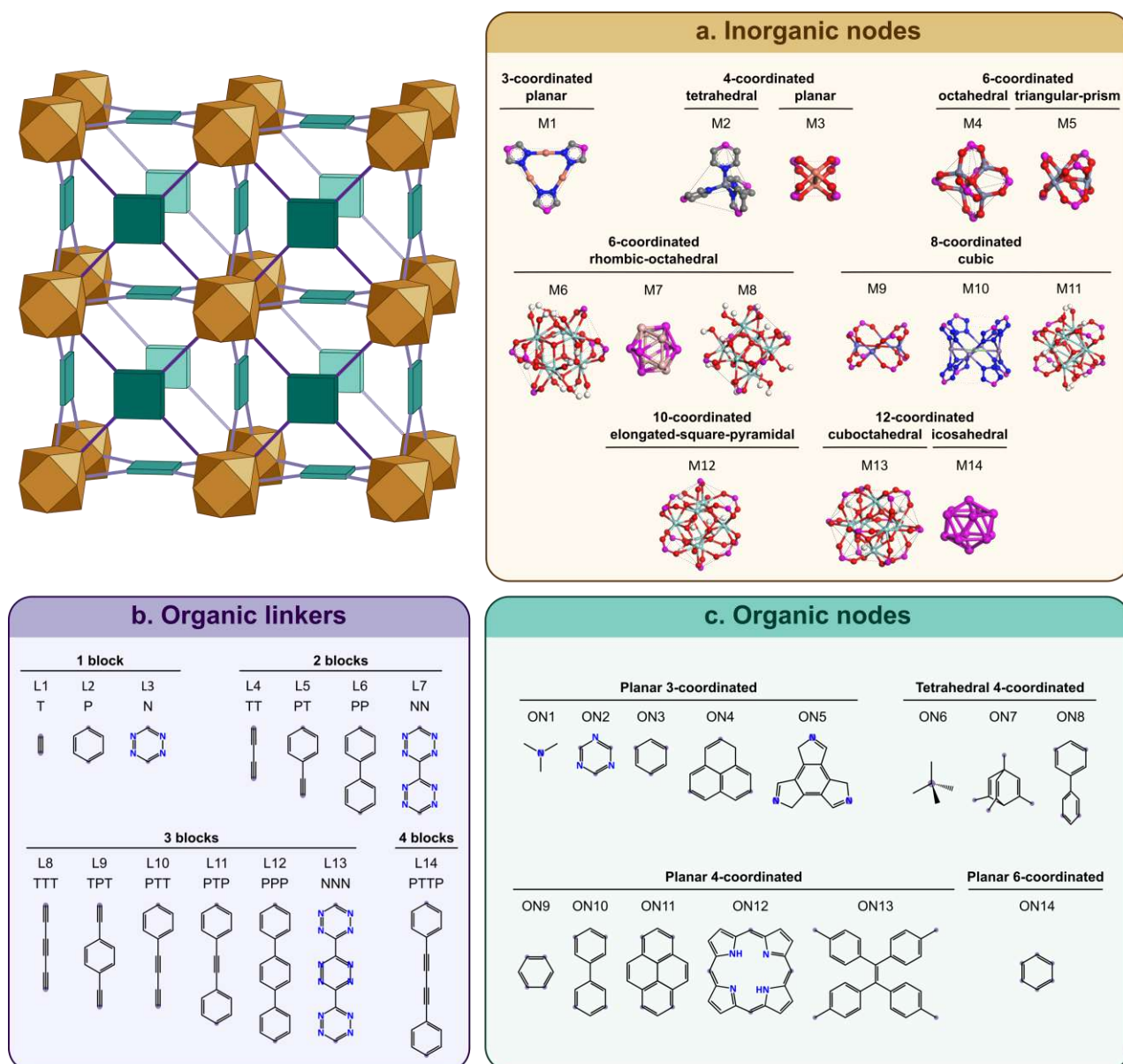
Fig. 1. Building blocks used to construct the subset of 3,385 MOFs containing 41 topologies. The top left Figure shows an example topological blueprint; colors show different MOF building units in a-c**. a.** Organic linkers (L); triple bonds, phenyl rings, and nitrogenated-phenyl rings are denoted by T, P and N, respectively. **b.** Organic nodes (ON) and **c.** Inorganic nodes (M). The numbers are used as identifiers. The purple circles represent connecting points to other building blocks.

High-throughput calculations of mechanical properties in MOFs: structure-stability relationships. Figure 2 shows the correlation between the bulk modulus (K) and the largest cavity diameter (LCD). The LCD is in turn correlated with other structural properties such as the pore volume, void fraction, surface area and density. General trends similar to the ones observed here between the bulk modulus and the LCD were also found between the shear modulus and the LCD (Fig. S3). All structures with $K > 30$ GPa have an LCD < 30 Å, whereas at LCD values < 20 Å, a wide spread of K values (0-140 GPa) can be observed. To shed light on the importance of topology on the mechanical robustness of certain structures, we

added another dimension to the *K* versus LCD representation and highlighted selected topologies for comparison (Fig. 2). Even for structures having the same LCD (e.g. see LCD = 10 or 15 Å), a quite large spread of the *K* values is observed depending on the topology. In other words, certain topologies have higher or lower bulk moduli irrespective of their pore size. For example, *pth* and *spn* topologies – highlighted in green and blue and for instance encountered in CMOF-1 and MOF-808 – show low *K* values across all pore sizes, whereas *fcu* (e.g. UiO-66), *reo* (e.g. DUT-51) and *ftw* (e.g. NU-1100) consistently present stiffer structures at similar pore size ranges. While the *ith* topology, encountered e.g. in DUT-78, has some of the highest bulk moduli found in MOFs, even comparable to those of zeolites,(Evans and Coudert, 2017) it is outperformed by many other topologies when considering structures with an LCD > 5 Å (e.g. at a LCD of 10 Å *fcu* MOFs show higher *K* values than *ith* MOFs).

Although the large datasets presented in Figure 2 clearly correlate the mechanical properties of MOFs with their LCD and topology, it is thus far not clear how various structural complexities – linker length, volumetric and gravimetric surface area, density, node coordination characteristics, void fraction, pore volume, pore limiting diameter (PLD), LCD, and PLD/LCD ratio – contribute to the MOFs' mechanical behavior and how these structural-mechanical stability relations are correlated with the topology. To obtain insights into these subtle dependencies, we developed an interactive visualization tool to explore the structure-mechanical stability relationships with the key advantage that users can examine how these 12 MOF structural features and, most importantly, topology determine the mechanical properties. With the aim to provide strategies to improve MOFs' mechanical stability, the web-based tool we developed is capable of presenting the structure-mechanical stability landscape of MOFs considering 15 descriptors along 5 dimensions: see http://aam.ceb.cam.ac.uk/mof-explorer/mechanicalproperties, allowing to filter the data or to zoom in on a specific area of the graphical representations, and the Supplementary Video 1 for more details.
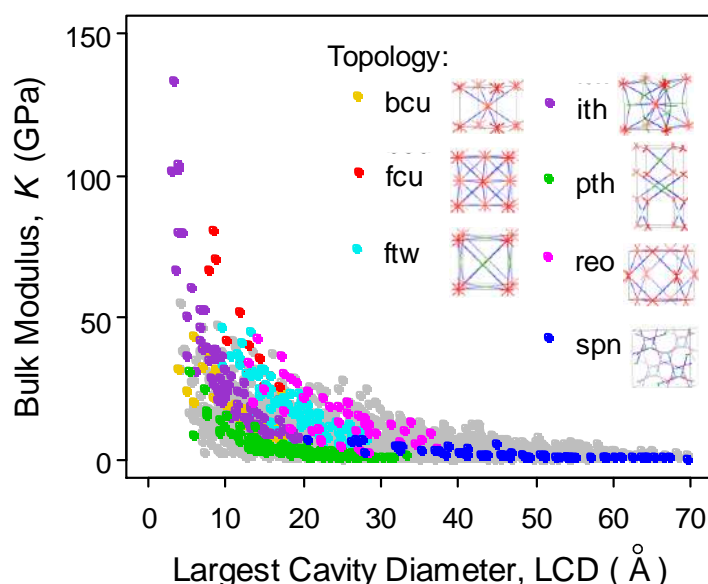
Fig. 2. High-throughput simulations of mechanical properties of MOFs. Bulk modulus (K) is plotted versus the largest cavity diameter (LCD) for 3,385 MOFs. Selected topologies are highlighted by different colors; all other topologies are shown in light grey. Each point represents a different MOF.

Hereafter, the tool is used to explore what makes certain topologies more robust than others and how this is affected by particular choices of key structural features such as organic linker length and type as well as the coordination environment between inorganic nodes and organic nodes or linkers. Some structures consist of both metal-based and organic nodes that show different coordination numbers; as such, we used in our analysis the maximum coordination number (MCN) of these two values. To begin, we examined the effect of the linker length – which is generally associated with the void fraction and pore volume – on the bulk modulus. Figure 3a shows K values versus LCD with structures containing 1 (green), 2 (yellow) and 3 phenyl rings (cyan) highlighted in the dataset. Clearly, frameworks containing one phenyl block, generally associated with narrower porosities and limited pore volumes, confer higher mechanical strength relative to those with longer linkers, e.g. structures with 2 or 3 phenyl rings. Similar trends were observed for structures containing triple bonds and nitrogenated linkers (Figs. S4-S5). To further emphasize on this finding, we highlighted two well-known series of MOFs belonging to the *fcu* and *pcu* topologies: the zirconium-based UiO-66 and zinc-based IRMOF-type materials, respectively. In agreement with the general trend observed for the highlighted structures with increasing number from 1 to 3 phenyl rings, there is a decrease in the bulk moduli for IRMOF-1, -10 and -16 and more prominently for UiO-66, -67 and -68. This finding suggests that shortening or expanding ligands in certain topologies presents more significant changes

in the MOFs' mechanical properties, confirming the earlier theoretical results that focused on the UiO-66 series.(Rogge et al., 2016b; Wu et al., 2013)

Figure 3b shows how the K values correlate with the MCN of the MOF. Structures with an MCN of 12 dominate the high bulk modulus space, whereas structures with an MCN of 8 and 4 have lower bulk moduli. This shows how resistance to mechanical forces is highly influenced by the number of node connections. Physically, topologies with low-coordinated nodes (e.g. *bor, pth, pts* and *tbo*; Fig. 3) have bond angles that can potentially flex with relative ease, allowing the frameworks to accommodate for stress and deform under pressure and shear (Fig. S3), whereas highly-coordinated topologies (e.g. *ith, fcu* and *ftw*; Fig. 3) are less flexible and thus changes in bond angles and lengths are associated with higher energy costs. This observation was recently exploited to stabilize MOFs via retrofitting.(Kapustin et al., 2017) It is noteworthy that high-K MOFs – characterized by structures with high coordination numbers – are dominated by materials with zirconium cuboctahedral nodes (e.g. M13 in Fig. 1a) such as those present in the UiO-66 family. In addition to the high coordination number of the nodes, zirconium-based MOFs have been previously reported to render superior mechanical stability due to the strong oxophylic character of zirconium, leading to strong zirconium-oxygen bonds.(Howarth et al., 2016; Rogge et al., 2018) Fig. S6 shows that variations between bulk moduli exist among topologies containing the same MCN. For example, for MCN = 12, *fcu* presents higher bulk moduli over *ftw* and *ith* topologies for MOFs with 10 Å < LCD < 20 Å. For the same range of LCD values, *reo* and *csq* for MCN = 8 and *pto* for MCN = 4 show higher bulk moduli compared with other topologies. The web-based visualization tool can also be used to determine the mechanical properties in terms of other specific structural properties such as the surface area of the MOFs. The latter is a key factor in determining the potential of these materials for energy applications for which their gas adsorption capacity is a central quantity. Figure 3c shows that although dense structures with very low surface areas (purple points) close to zero are mechanically very robust, they probably would exhibit limited adsorption capacities. MOFs with surface areas of 1,000–3,000 m^2/g and densities of 0.5–1 g/cm^3 (light blue and green points) can relatively confer high mechanical strength while maintaining good adsorptive characteristics, a combination which makes them more appealing for energy applications. Open structures with low densities and very high surface areas (> 7,000 m^2/g) show extremely low mechanical strength and are therefore of only limited relevance for industrial applications.
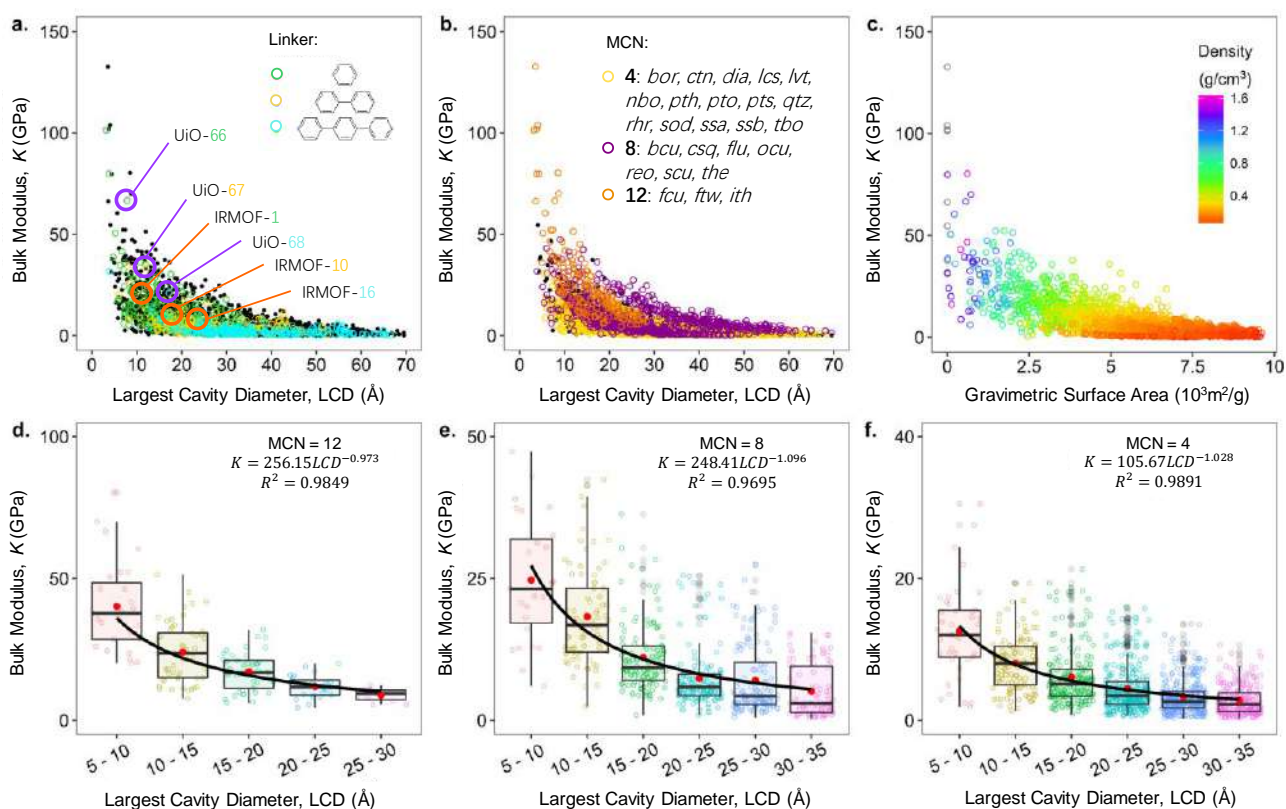
Fig. 3. Structure-stability relationships in MOFs. Bulk modulus, *K*, versus the largest cavity diameter (LCD) for 3,385 MOFs. Colored **a.** structures with one, two and three phenyl rings (selected common MOFs containing phenyl rings are highlighted in the dataset); **b.** structures and topologies with maximum coordination numbers (MCN) of 4, 8 and 12; filled black circles represent all other MOFs in a. and b. **c.** Bulk modulus, *K*, versus the gravimetric surface area; the color code represents the MOFs' density. **d-f** Box and whisker plots comparing bulk modulus changes with LCD for different maximum coordination numbers.

To quantitatively analyze whether the linker length or the coordination number and topology is a more important descriptor in determining the mechanical stability, we compared the *K* values for structures with MCN 12, 8 and 4 with respect to their LCD (Figs. 3d-f). The absolute values and the variation of the bulk moduli for each MCN at different pore sizes are remarkable. For 5 Å < LCD < 10 Å, average *K* values are 40, 25 and 15 GPa for MCNs amounting to 12, 8 and 4, respectively. For MCN=12, there is a considerably steeper decrease in bulk modulus as the pore size increases compared with MCN=8 and MCN=4. For the lowest MCN of 4, the bulk modulus decreases only slightly as the pore size increases. These trends indicate that the expansion of the organic linkers induces more drastic changes in mechanical stability decay for network topologies with high coordination numbers such as *ith*, *fcu* and *ftw*, explaining why these effects have been predominantly observed in the UiO-66 series exhibiting the *fcu* topology.(Rogge et al., 2016b; Wu et al., 2013) Furthermore, structures consisting of only triple-bond linkers (e.g. L1/L4/L8 in Fig. 1b) tend to have slightly higher bulk moduli than those with only phenyl rings – while variations

exist within the dataset (Fig. S7a). When linkers containing both phenyl ring and triple-bond blocks are considered, our high-throughput calculations do not show any appreciable differences between different positions of e.g. phenyl rings in the linker and MOFs mechanical properties (Fig. S7b). This point is fully addressed later in this work, where molecular dynamics calculations based on accurate *ab initio*-based force fields are performed for selected materials.

To obtain a more systematic insight into the correlations between the aforementioned 13 geometrical descriptors, including the topology, and the mechanical stability of MOFs, we evaluated the predictability of the bulk modulus using an artificial neural network (ANN) – a machine learning algorithm known for its ability to reproduce and model nonlinear processes.(Conduit et al., 2017; Verpoort et al., 2018) The ANN inputs all of the design variables, geometrical and topological, of the MOFs to predict the mechanical properties; mathematical details are described in the Methods. We used the ANN to predict the bulk modulus for all the MOFs in our dataset considering two scenarios. In the first case, we used a combination of four MOF structural descriptors: density, gravimetric surface area, LCD and void fraction. In the second case, we also took into account the topology as a descriptor. The parity plot in Figure 4a compares the simulated bulk moduli with those predicted with the ANN for the model without topological descriptors. The data are scattered in the entire range of K values, yielding a high coefficient of determination (R^2) of 0.70, measured by five-fold cross-validation. In contrast, when the model is trained with topological information (Fig. 4b), the R^2 was significantly improved to 0.98, further evidencing that topological features are highly correlated to the mechanical properties of MOFs and are essential to accurately predict the bulk modulus. The box plots in Figure 4c and Figure 4d quantify the variations of the ANN predicted K values from the parity line (i.e. perfect agreement). The variation of the absolute difference spread in the interquartile range (IQR, i.e. the box height) and the skew of the data points are particularly interesting. The model trained without topological descriptors obtains the least accuracy for high K materials, as shown by the increased interquartile height for e.g. the 40-60 GPa range (Fig. 4c). In stark contrast, the model that takes into account the topology delivers the best accuracy for the same range of high K structures where data points lie close to the parity line (Fig. 4d). The clear advantage of the ANN approach used here is that predictions for mechanical properties are readily available for other existing MOFs as well as for MOFs to be synthesized in the future. In these cases, one only needs the easily accessible descriptors employed here – topology, density, gravimetric surface area, LCD and void fraction – to quickly and qualitatively pinpoint where the structure of interest lies in the structure-stability landscape of MOF materials without the

need for further calculations. The ANN approach therefore substantially decreases the effort needed to design new MOFs exhibiting an elevated stability, crucial for industrial applications.
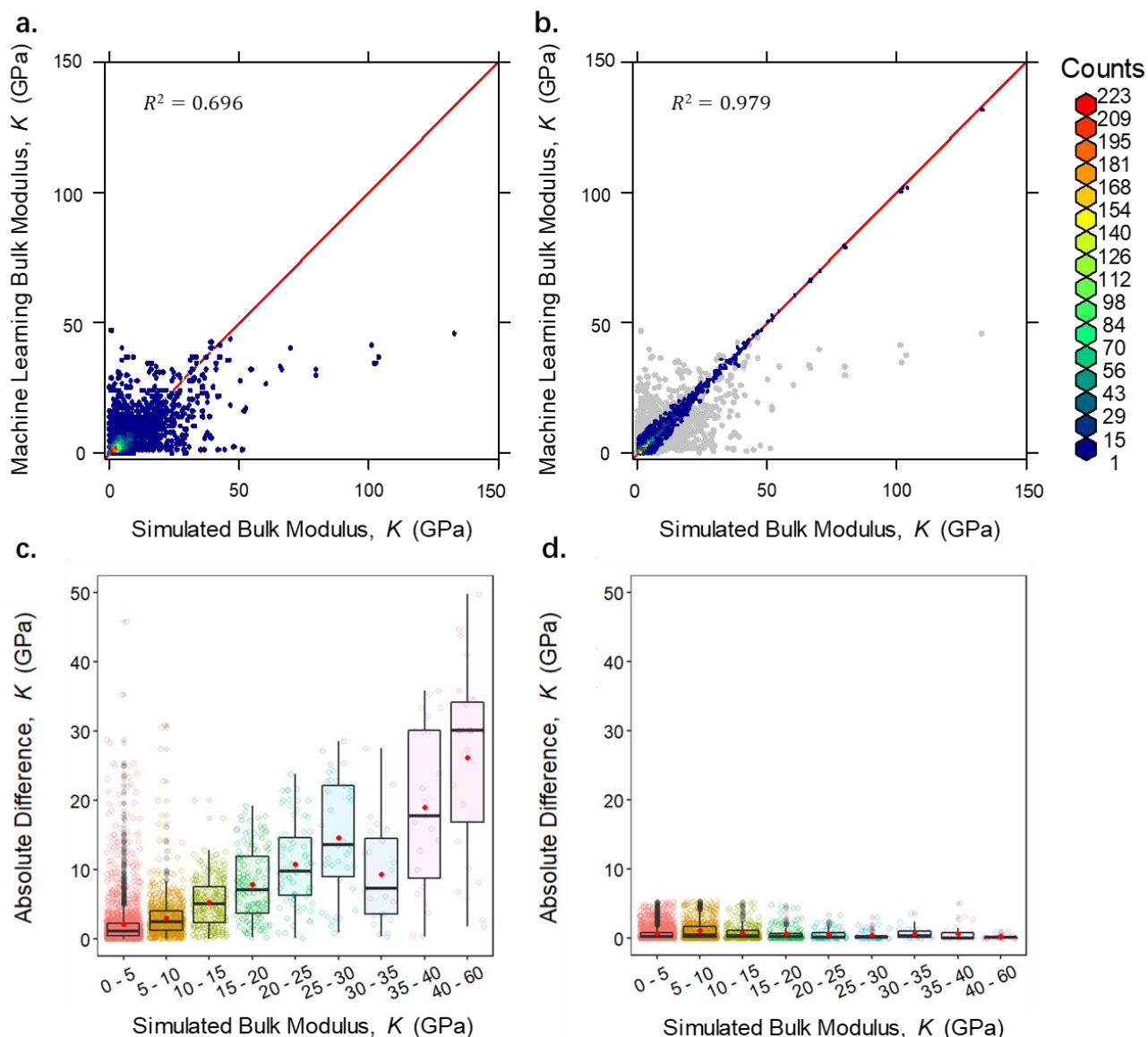
Fig. 4. Evaluation of machine learning in predicting mechanical properties in MOFs. Parity plots for machine learning predicted versus simulated bulk modulus using density, void fraction, gravimetric surface area and LCD without **a.** and with **b.** topological descriptors. The color scale indicates the number of MOFs that have the corresponding result in **a.** and **b.**; The red diagonal is the parity line. The grey points in the background in **b.** correspond to the data obtained without topological descriptors. **c.** and **d.** Boxplots of the "vertical distance" between a point and the corresponding point on the parity line in the **a.** case and **b.** case.

Mechanical behavior of selected materials under operando conditions. The high-throughput simulations performed so far rely on fast calculations of mechanical properties at 0 K and at equilibrium, revealing clear structural-mechanical property trends for a diverse set of MOF topologies. However, these fast calculations cannot precisely describe the

mechanical behavior of MOF structures when subtle differences in the organic linker chemistry are applied. Good examples of such subtleties are those cases where the non-functionalized ligand chemistry is changed, e.g. from a triple bond to a phenyl ring or to various combinations/orders of both moieties. Furthermore, it is crucial to investigate whether the equilibrium properties extracted from the 0 K simulations above can easily be generalized to account for the finite temperatures and pressures present under *operando* conditions which may be far from equilibrium. Addressing these questions requires a more advanced approach, relying on the construction of mechanical equations of state which allow us to determine the mechanical properties at finite temperatures and deduce the loss-of-crystallinity pressure.(Rogge et al., 2015; Rogge et al., 2018; Rogge et al., 2016a; Vanduyfhuys et al., 2018a)

The approach is illustrated here for a subset of the high-throughput space bearing the *fcu* topology, encountered in UiO-66-type materials, for which our prior HTS indicated an outstanding mechanical stability while maintaining an appreciable LCD and pore volume, necessary for energy applications for which a good adsorption performance and mechanical stability are needed. Through molecular dynamics (MD) simulations using *ab initio*-derived QuickFF force fields,(Vanduyfhuys et al., 2015) 300 K pressure-versus-volume equations of state are constructed to accurately determine the mechanical stability of those MOFs composed of the 12-coordinated $Zr_6(\mu_3-O)_4(\mu_3-OH)_4$ metal-oxide nodes and each of the fourteen different organic ligands depicted in Figure 1b, adopting the protocol outlined in Ref.(Rogge et al., 2016a) The chosen linkers, containing up to four phenyl, carbon-carbon triple bond and/or tetrazine moieties, form a representative set to study the effect of replacing or reordering these moieties on the mechanical properties of the fourteen MOFs. A first comparison of the predicted equilibrium cell lengths at 300 K with the measured ones for the MOFs that were already characterized experimentally – the UiO-66 series,(Cavka et al., 2008) NU-800,(Gomez-Gualdron et al., 2014) BUT-30,(Lv et al., 2015) and PCN-111(Stewart et al., 2017) – reveals that our methodology yields a maximum deviation of only 2.6% for NU-800, while all other deviations are below 1.2% (see Table S3).

Given this good agreement, the equilibrium cell length, equilibrium bulk modulus, and loss-of-crystallinity pressure were derived from our 300 K pressure-versus-volume equations of state following the procedure outlined schematically in Figure 5a. Focusing on the equilibrium regime, Figure 5c reveals that the bulk modulus strongly decreases when adding extra moieties to the linker, similar to our earlier observation on the larger set of materials. These results also allow to further study the dependency of the bulk modulus at finite temperature on subtle differences in the nature and length of the organic linkers. When

looking at a fixed total number of moieties in the linker, exchanging a carbon-carbon triple bond (T) moiety with a phenyl (P) moiety leads to a decrease in the bulk modulus.
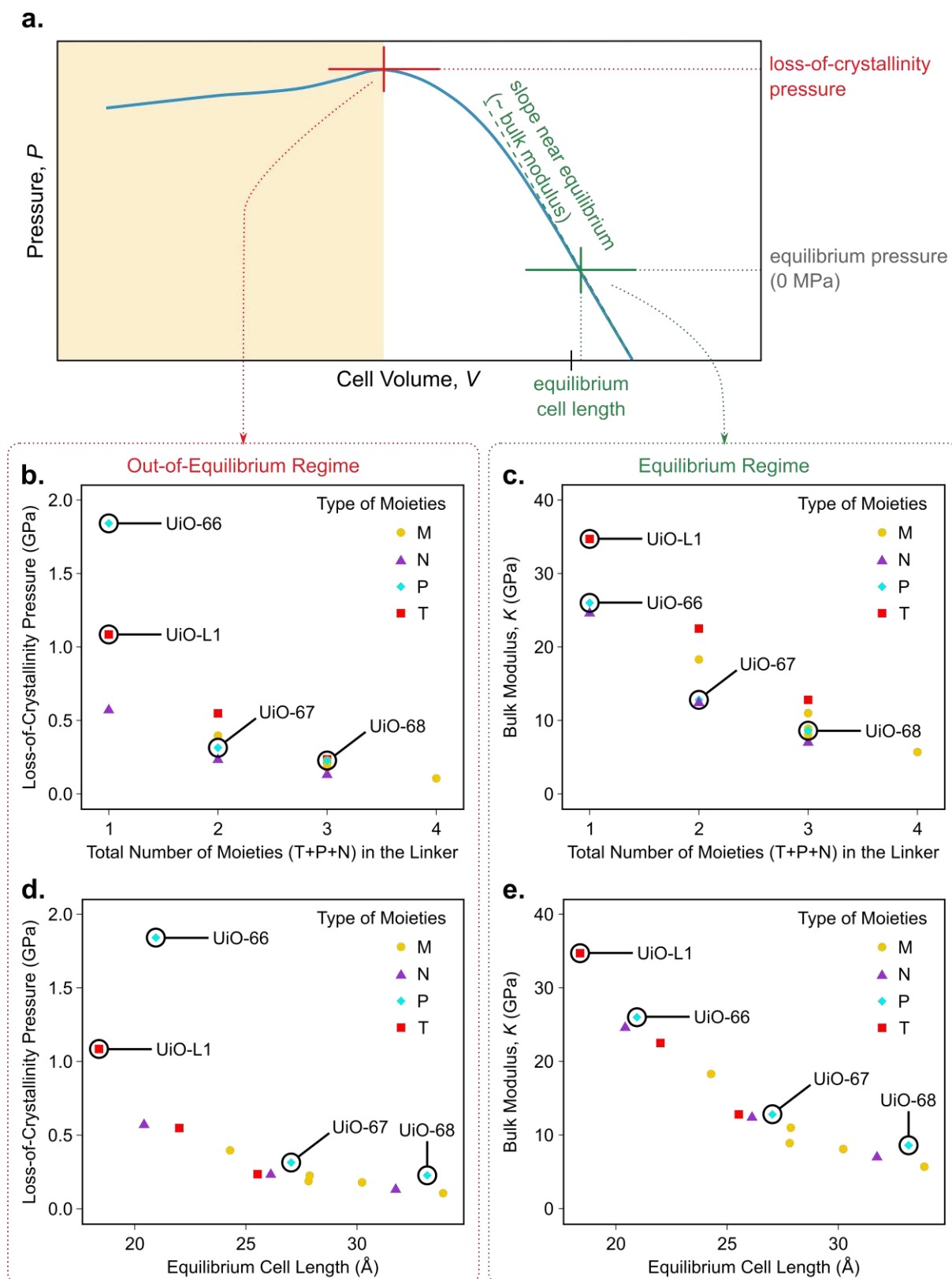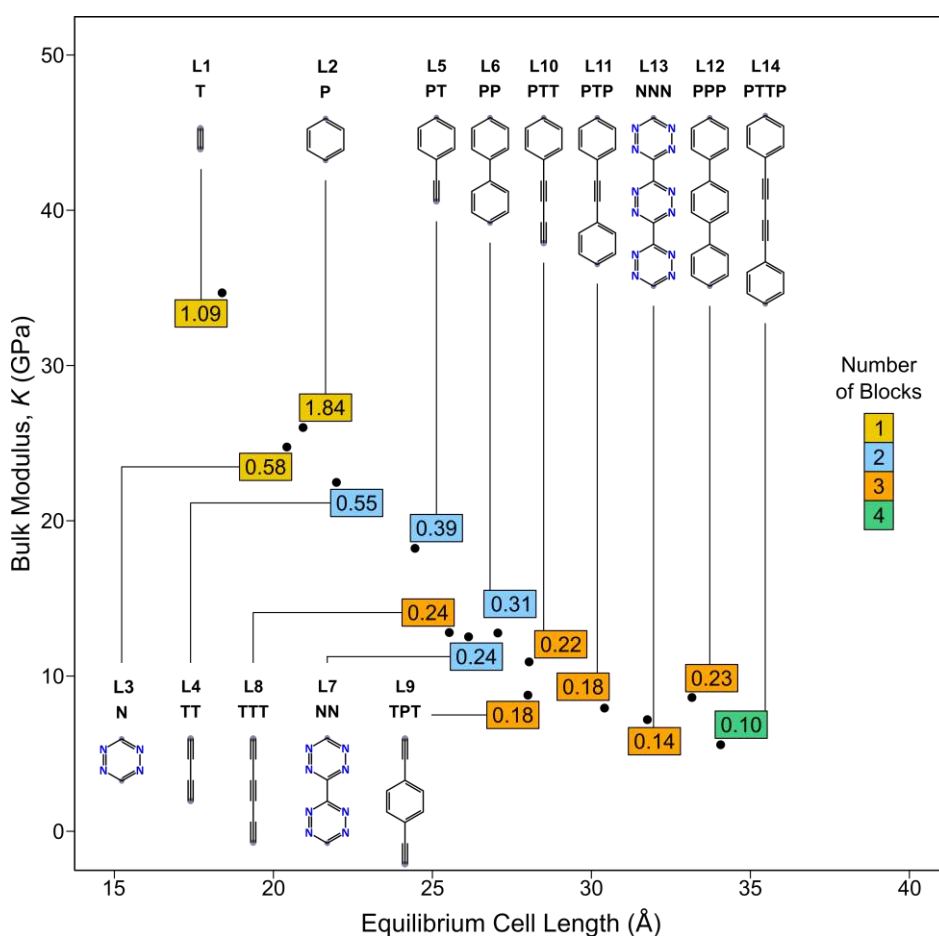

Fig. 5. Probing MOF stability using *operando* molecular dynamics. a. Schematic overview of the different structural and mechanical properties that can be extracted from the pressure-versus-volume equations of state at *operando* conditions. Predicted **b.** loss-of-crystallinity-pressure and **c.**

bulk modulus for the fourteen *fcu* materials as a function of the total number of moieties (T+P+N) in the organic linker; predicted **d.** loss-of-crystallinity pressure and **e.** bulk modulus as a function of the predicted equilibrium cell length of the MOF. Data points are color-coded according to the type of moieties in the linker, with linkers containing only T, P, or N indicated by red, cyan, and magenta spheres, respectively, and mixed M (T, P) linkers indicated with yellow spheres.

Furthermore, Figure 5c reveals that substituting the phenyl ring (P) by a tetrazine ring (N) leads to a consistent, albeit small reduction in the bulk modulus. These observations can be rationalized by determining the predicted bulk modulus as a function of the predicted equilibrium cell length (Fig. 5e). A clear negative correlation between both is present, indicating that the equilibrium cell length can be used as an accurate predictor for the bulk modulus for a given topology, with an increasing cell length leading to a decrease in bulk modulus. This is in full agreement with the observations that the bulk modulus decreases with increasing LCD for the larger dataset in Figure 2, as the LCD and equilibrium cell length are linearly dependent for a given topology.

At this point, we mainly focused on equilibrium properties – the equilibrium cell length and bulk modulus – to extract information about the mechanical rigidity of these materials. However, for MOFs to be routinely adopted for industrial applications, we are especially interested in the pressure these materials can withstand before collapsing towards an amorphous phase, as this determines the maximum pressure they can withstand during pelletization or when used in large adsorbent beds. From the pressure-versus-volume equations of state, it is straightforward to derive the loss-of-crystallinity pressure, which was validated to be an accurate proxy for the experimental amorphization pressure.(Rogge et al., 2016a) Figures 5b and 5d show the predicted loss-of-crystallinity pressure as a function of the total number of moieties in the linker and as a function of the equilibrium cell length, respectively. Only UiO-66 and UiO-L1 retain their crystal structures above 1 GPa. The *fcu* MOFs with longer linkers (e.g. linkers containing 2-4 moieties) are clearly less stable with loss-of-crystallinity pressures below 0.55 GPa. As highlighted in Figure 6, we observe that the exact position of the phenyl moiety does not appreciably influence the mechanical stability, as the *fcu* MOFs based on linkers L9, L10 and L11 have a comparable bulk modulus. For most materials, a good correlation between the predicted bulk modulus at equilibrium and the predicted loss-of-crystallinity pressure near mechanical instability is observed (Fig. 6). Therefore, for a specific topology, the equilibrium cell length seems to be a good predictor of mechanical stability, both at equilibrium, as expressed via the bulk modulus, and near mechanical instability, as expressed via the loss-of-crystallinity pressure. This conclusion is in agreement with the HTS results described above. However, one material deviates strongly from this global trend: whereas the phenyl-based UiO-66 (linker

14

L2) has an appreciable larger equilibrium cell length than its triple-bond counterpart UiO-L1 (linker L1) and an associated smaller bulk modulus (34.7 GPa versus 26.0 GPa), its loss-of-crystallinity pressure is substantially larger (1.84 GPa versus 1.09 GPa). For the two materials, also the Born stability criteria were constructed,(Born, 1940) to obtain insight into the macroscopic mode along which the material first becomes mechanically unstable, yielding complementary insight to the pressure-versus-volume profiles derived above.(Rogge et al., 2018) This further analysis learns that the exhibit a different weakest mode of deformation inducing the mechanical instability (see Fig. S22).

Fig. 6. Probing MOF stability using operando molecular dynamics. Predicted bulk modulus, equilibrium unit cell length, and loss-of-crystallinity pressure, as extracted from the 300 K pressure-versus-volume equations of state for fourteen *fcu* MOFs. Loss-of-crystallinity pressure is stated in the boxes. Box colors indicate the number of T, P or N blocks in the linker.

CONCLUSION

We have performed high-throughput molecular mechanics calculations to establish structure-mechanical stability relationships for 3,385 MOF materials with 41 distinct topologies. We not only identified top robust network topologies – crucial to design MOFs relevant for industrial applications – but also explained how the interplay between MOFs key

structural features, such as their building blocks coordination number and/or linker type and length, render more deformation-resistant structures. The web-based visualization tool allows users to analyze the results interactively through over 1000 unique structure-mechanical property relationships using 15 structural and mechanical features in 5D plots. This capability is key to understand the "combinatorial descriptors" that affect the mechanical stability of MOFs. In addition, we demonstrated the power of an artificial neural network algorithm to not only accurately predict the bulk modulus for a large number of materials, but also highlight the importance of taking into account the topology in the accuracy of such predictions. To obtain deeper molecular-level insight on the key features governing the mechanical stability of these materials and to investigate whether these 0 K HTS results can be generalized to finite temperature and pressures, *operando* MD simulations using *ab initio*-based force fields were performed for a representative set of 14 *fcu* MOFs. These MD simulations revealed that the equilibrium cell length and bulk modulus at 0 K, which can be obtained from a fast HTS, are representative of the critical pressure these materials can withstand at operando temperatures. As a result, this study provides unprecedented insight into the rational design of mechanically robust MOFs able to endure the pressures to which they are exposed in industrial settings. These capabilities will allow researchers to assess and easily predict the mechanical properties of new MOFs synthesized in their labs as well as to design hypothetical structures that combine good adsorption performances with an elevated mechanical stability, which is crucial for these materials to be adopted industrially in the energy domain and beyond.

PROCEDURES

High-throughput molecular mechanics calculations. For each MOF, we calculated the mechanical properties including the bulk, shear, and Young's moduli using classical molecular mechanics via the constant strain approach implemented in the Forcite module of Materials Studio.(Materials Studio User Manual; BIOVIA (Accelrys): San Diego) First, the geometry of the structures was optimized using the Universal Force Field (UFF), given its general applicability for determining the mechanical properties of rigid MOFs:(Boyd et al., 2017) see also Fig. S24. When dealing with Cu-Cu paddle-wheel structures, we kept a "scaffold" atom bound to Cu atom to keep it 6-coordinated in the paddlewheel environment so the MOFs retain their structural integrity. We also compared the UFF predicted elastic constants for 14 *fcu*-type materials with those obtained with *ab initio*-based force fields with QuickFF.(Vanduyfhuys et al., 2015) From Table S5 and Figure S24, it is clear that the UFF force field in Materials Studio correctly predicts the trends of the elastic constants as a

function of the linkers, although the absolute values of the elastic constants are overestimated by up to about a factor of 2-3 compared to the results obtained with QuickFF. Such qualitative agreement was deemed satisfactory for the first stage of our HTS approach for thousands of materials. In Materials Studio, any symmetry from the MOF was removed and different strains were applied to the structure. For each strain, the structure was re-optimized (with the relevant constraints) and the stress was calculated. The obtained stress and strain tensors were used to determine the mechanical properties that show the material response to deformation (see Supplementary Information for details).(Materials Studio User Manual; BIOVIA (Accelrys): San Diego) Table S1 shows all the simulation parameters. Structural characteristics including accessible surface area, accessible volume, largest cavity diameter (LCD), and pore limiting diameter (PLD) were computed using the Zeo++ software package.(Willems et al., 2012) A N_2-equivalent probe of radius 1.86 Å was used for surface area calculations, whereas a probe of radius 0 Å was used for calculating the pore volume. Fig. S2 shows the histograms of the geometric properties for all MOFs.

Machine learning algorithm. The tool and methodology follow the prescription developed by Conduit *et al.*(Conduit et al., 2017; Verpoort et al., 2018) A typical artificial neural network (ANN) is shown in Scheme 1. The I inputs x_i for $i=1...I$ are used to calculate H intermediate hidden nodes η_h for $h=1...H$. The free parameters A_{ih}, B_h, C_h, D are optimized to predict training data y through a non-linear tanh function, and then verified against 20% of the data that was withheld for cross-validation. The mathematical transformation contains weights that are optimized during the training process with the training data (i.e. 80% of the total data available). The procedure was repeated five times during cross-validation. Typically, thirty hidden nodes gave the best fitting neural network. Starting from the simulated bulk modulus, an ANN model is trained on the 3,385 MOF structures data to predict the bulk modulus for a given set of geometrical properties and optional topology. The model without topological information uses 4 descriptors, whereas the model with topologies employs 45 to include each of the 41 topologies as a separate descriptor corresponding to having or not having a certain topology (for example, a descriptor *fcu* has the value of 1 for all MOF structures of *fcu* topology and a value of 0 for all other structures). The topology is treated as 41 separate categories as they cannot be placed in an ordered list.
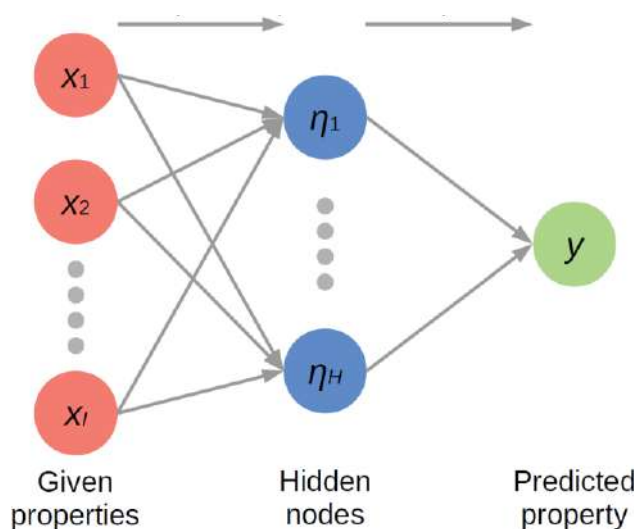
Scheme 1. The artificial neural network (ANN). The graph shows how the output *y* is computed from all the inputs x_i. A linear combination (grey lines) of the given properties (red) are taken by the hidden nodes (blue), a non-linear tanh function, and a linear combination (grey lines) gives the predicted property (green).

Molecular dynamics simulations with *ab initio* derived force fields. Following the large screening, MD simulations on the materials exhibiting the *fcu* topology were carried out in Yaff, a freely available, in-house developed, software package. These finite-temperature simulations were performed using newly developed force fields based on accurate *ab initio* input following the QuickFF protocol,(Vanduyfhuys et al., 2015; Vanduyfhuys et al., 2018b) using the conventional unit cell containing four inorganic nodes. For UiO-66, it was validated earlier that this conventional unit cell is sufficiently large to reliably predict its mechanical stability.(Rogge et al., 2016a) The mechanical properties at finite temperature were determined via the construction of pressure-versus-volume equations of state for the fourteen *fcu* materials, carried out in the dedicated $(N, V, \sigma_a = 0, T)$ ensemble.(Rogge et al., 2015) This ensemble was specifically constructed to study phase transformations and mechanical instability for materials in which the volume is a good descriptor of the phase transition.(Rogge et al., 2015) Figs. S8-S21 show the resulting profiles, from which the structural and mechanical properties both at equilibrium and near mechanical instability were extracted. To predict the experimental loss-of-crystallinity pressure from our simulations with periodic boundary conditions, we extracted the critical pressure above which the predicted symmetry of the material drops sharply. Further details on these MD simulations can be found in the Supplementary Information.

5D web-domain visualization tool. Further to the mechanical properties analysis, we have established a 5D interactive visualization web-domain. All the structure-stability relationships discussed in this paper can be reproduced online at

Supplemental information

Supplemental Information includes simulation procedures, the artificial neural network code for MOFs' mechanical properties predictions and a video (dynamic exploration of the 5D web-domain visualization tool-mechanical properties).

Acknowledgements

Author contributions

Conceptualization, P. Z. M. and D. F-J.; Investigation, P. Z. M., A. L., C.-M. C., G. C., M. A.-A., A. L., S. M. J. R. and J. W.; Formal Analysis P. Z. M., S. M. J. R., V. V. S., N. M., D. G-G. and D. F-J. Resources, V. V. S. and D. F.-J. Writing – Original Draft, P. Z. M., S. M. J. R., C.-M. C., A. L. and D. F-J.; Writing – Review & Editing, all the authors. Supervision, P. Z. M., V. V. S., D. F.-J.

Declaration of interests

D.F.-J. has a financial interest in the start-up company Immaterial Labs, which is seeking to commercialize metal-organic frameworks. The authors declare no other competing interests.

References

Alexandrov, E.V., Blatov, V.A., Kochetkov, A.V., and Proserpio, D.M. (2011). Underlying nets in three-periodic coordination polymers: topology, taxonomy and prediction from a computer-aided analysis of the Cambridge Structural Database. CrystEngComm *13*, 3947-3958.

Bernini, M.C., Fairen-Jimenez, D., Pasinetti, M., Ramirez-Pastor, A.J., and Snurr, R.Q. (2014). Screening of bio-compatible metal-organic frameworks as potential drug carriers using Monte Carlo simulations. J Mater Chem B *2*, 766-774.

Bobbitt, N.S., Mendonca, M.L., Howarth, A.J., Islamoglu, T., Hupp, J.T., Farha, O.K., and Snurr, R.Q. (2017). Metal-organic frameworks for the removal of toxic industrial chemicals and chemical warfare agents. Chem Soc Rev *46*, 3357-3385.

Born, M. (1940). On the stability of crystal lattices. I. Math Proc Cambridge Philos Soc *36*, 160-172.

Boyd, P.G., Moosavi, S.M., Witman, M., and Smit, B. (2017). Force-Field Prediction of Materials Properties in Metal-Organic Frameworks. J Phys Chem Lett *8*, 357-363.

Burtch, N.C., Heinen, J., Bennett, T.D., Dubbeldam, D., and Allendorf, M.D. (2018). Mechanical Properties in Metal–Organic Frameworks: Emerging Opportunities and Challenges for Device Functionality and Technological Applications. Adv Mater, 1704124.

Cavka, J.H., Jakobsen, S., Olsbye, U., Guillou, N., Lamberti, C., Bordiga, S., and Lillerud, K.P. (2008). A New Zirconium Inorganic Building Brick Forming Metal Organic Frameworks with Exceptional Stability. J Am Chem Soc *130*, 13850-13851.

Colón, Y.J., Fairen-Jimenez, D., Wilmer, C.E., and Snurr, R.Q. (2014). High-Throughput Screening of Porous Crystalline Materials for Hydrogen Storage Capacity near Room Temperature. J Phys Chem C *118*, 5383-5389.

Conduit, B.D., Jones, N.G., Stone, H.J., and Conduit, G.J. (2017). Design of a nickel-base superalloy using a neural network. Mater Des *131*, 358-365.

Coudert, F.-X., and Fuchs, A.H. (2016). Computational characterization and prediction of metal–organic framework properties. Coord Chem Rev *307*, 211-236.

Evans, J.D., and Coudert, F.-X. (2017). Predicting the Mechanical Properties of Zeolite Frameworks by Machine Learning. Chem Mater *29*, 7833-7839.

Faust, T. (2015). Nanomedicine: MOFs deliver. Nat Chem *7*, 270-271.

Furukawa, H., Cordova, K.E., O'Keeffe, M., and Yaghi, O.M. (2013). The Chemistry and Applications of Metal-Organic Frameworks. Science *341*, 123044.

Gómez-Gualdrón, D.A., Colón, Y.J., Zhang, X., Wang, T.C., Chen, Y.-S., Hupp, J.T., Yildirim, T., Farha, O.K., Zhang, J., and Snurr, R.Q. (2016). Evaluating topologically diverse metal-organic frameworks for cryo-adsorbed hydrogen storage. Energy Environ Sci *9*, 3279-3289.

Gomez-Gualdron, D.A., Gutov, O.V., Krungleviciute, V., Borah, B., Mondloch, J.E., Hupp, J.T., Yildirim, T., Farha, O.K., and Snurr, R.Q. (2014). Computational Design of Metal–Organic Frameworks Based on Stable Zirconium Building Units for Storage and Delivery of Methane. Chem Mater *26*, 5632-5639.

Hajek, J., Caratelli, C., Demuynck, R., De Wispelaere, K., Vanduyfhuys, L., Waroquier, M., and Van Speybroeck, V. (2018). On the intrinsic dynamic nature of the rigid UiO-66 metal-organic framework. Chem Sci *9*, 2723-2732.

Horcajada, P., Chalati, T., Serre, C., Gillet, B., Sebrie, C., Baati, T., Eubank, J.F., Heurtaux, D., Clayette, P., Kreuz, C., *et al.* (2010). Porous metal-organic-framework nanoscale carriers as a potential platform for drug delivery and imaging. Nat Mater *9*, 172-178.

Horike, S., Shimomura, S., and Kitagawa, S. (2009). Soft porous crystals. Nat Chem *1*, 695-704.

Howarth, A.J., Liu, Y., Li, P., Li, Z., Wang, T.C., Hupp, J.T., and Farha, O.K. (2016). Chemical, thermal and mechanical stabilities of metal–organic frameworks. Nat Rev Mater *1*, 15018.

Kapustin, E.A., Lee, S., Alshammari, A.S., and Yaghi, O.M. (2017). Molecular Retrofitting Adapts a Metal–Organic Framework to Extreme Pressure. ACS Central Science *3*, 662-667.

Li, J.-R., Kuppler, R.J., and Zhou, H.-C. (2009). Selective gas adsorption and separation in metal-organic frameworks. Chem Soc Rev *38*, 1477-1504.

Lv, X.-L., Tong, M., Huang, H., Wang, B., Gan, L., Yang, Q., Zhong, C., and Li, J.-R. (2015). A high surface area Zr(IV)-based metal–organic framework showing stepwise gas adsorption and selective dye uptake. J Solid State Chem *223*, 104-108.

Mason, J.A., Oktawiec, J., Taylor, M.K., Hudson, M.R., Rodriguez, J., Bachman, J.E., Gonzalez, M.I., Cervellino, A., Guagliardi, A., Brown, C.M.*, et al.* (2015). Methane storage in flexible metal–organic frameworks with intrinsic thermal management. Nature *527*, 357-361.

Materials Studio User Manual; BIOVIA (Accelrys): San Diego, C.

Maurin, G., Serre, C., Cooper, A., and Férey, G. (2017). The new age of MOFs and of their porous-related solids. Chem Soc Rev *46*, 3104-3107.

Miller, S.E., Teplensky, M.H., Moghadam, P.Z., and Fairen-Jimenez, D. (2016). Metal-organic frameworks as biosensors for luminescence-based detection and imaging. Interface Focus *6*, 20160027.

Moghadam, P.Z., Fairen-Jimenez, D., and Snurr, R.Q. (2016). Efficient identification of hydrophobic MOFs: application in the capture of toxic industrial chemicals. J Mater Chem A *4*, 529-536.

Moghadam, P.Z., Ivy, J.F., Arvapally, R.K., dos Santos, A.M., Pearson, J.C., Zhang, L., Tylianakis, E., Ghosh, P., Oswald, I.W.H., Kaipa, U.*, et al.* (2017a). Adsorption and molecular siting of CO2, water, and other gases in the superhydrophobic, flexible pores of FMOF-1 from experiment and simulation. Chem Sci *8*, 3989-4000.

Moghadam, P.Z., Li, A., Wiggin, S.B., Tao, A., Maloney, A.G.P., Wood, P.A., Ward, S.C., and Fairen-Jimenez, D. (2017b). Development of a Cambridge Structural Database Subset: A Collection of Metal–Organic Frameworks for Past, Present, and Future. Chemistry of Materials *29*, 2618-2625.

Moosavi, S.M., Boyd, P.G., Sarkisov, L., and Smit, B. (2018). Improving the Mechanical Stability of Metal–Organic Frameworks Using Chemical Caryatids. ACS Central Science *4*, 832-839.

Ortiz, A.U., Boutin, A., Fuchs, A.H., and Coudert, F.-X. (2012). Anisotropic Elastic Properties of Flexible Metal-Organic Frameworks: How Soft are Soft Porous Crystals? Phys Rev Lett *109*, 195502.

Peterson, G.W., DeCoste, J.B., Glover, T.G., Huang, Y., Jasuja, H., and Walton, K.S. (2013). Effects of pelletization pressure on the physical and chemical properties of the metal–organic frameworks Cu3(BTC)2 and UiO-66. Micropor Mesopor Mater *179*, 48-53.

Rogge, S.M.J., Bavykina, A., Hajek, J., Garcia, H., Olivos-Suarez, A.I., Sepúlveda-Escribano, A., Vimont, A., Clet, G., Bazin, P., Kapteijn, F.*, et al.* (2017). Metal-organic and covalent organic frameworks as single-site catalysts. Chem Soc Rev *46*, 3134-3184.

Rogge, S.M.J., Vanduyfhuys, L., Ghysels, A., Waroquier, M., Verstraelen, T., Maurin, G., and Van Speybroeck, V. (2015). A Comparison of Barostats for the Mechanical Characterization of Metal–Organic Frameworks. J Chem Theory Comput *11*, 5583-5597.

Rogge, S.M.J., Waroquier, M., and Van Speybroeck, V. (2018). Reliably Modeling the Mechanical Stability of Rigid and Flexible Metal–Organic Frameworks. Acc Chem Res *51*, 138-148.

Rogge, S.M.J., Wieme, J., Vanduyfhuys, L., Vandenbrande, S., Maurin, G., Verstraelen, T., Waroquier, M., and Van Speybroeck, V. (2016a). Thermodynamic Insight in the High-Pressure Behavior of UiO-66: Effect of Linker Defects and Linker Expansion. Chem Mater *28*, 5721-5732.

Rogge, S.M.J., Wieme, J., Vanduyfhuys, L., Vandenbrande, S., Maurin, G., Verstraelen, T., Waroquier, M., and Van Speybroeck, V. (2016b). Thermodynamic Insight in the High-Pressure Behavior of UiO-66: Effect of Linker Defects and Linker Expansion. Chemistry of Materials *28*, 5721-5732.

Rubio-Martinez, M., Avci-Camur, C., Thornton, A.W., Imaz, I., Maspoch, D., and Hill, M.R. (2017). New synthetic routes towards MOF production at scale. Chem Soc Rev *46*, 3453-3480.

Sarkisov, L., Martin, R.L., Haranczyk, M., and Smit, B. (2014). On the Flexibility of Metal–Organic Frameworks. Journal of the American Chemical Society *136*, 2228-2231.

Sikora, B.J., Winnegar, R., Proserpio, D.M., and Snurr, R.Q. (2014). Textural properties of a large collection of computationally constructed MOFs and zeolites. Micropor Mesopor Mater *186*, 207-213.

Simon, C.M., Kim, J., Gomez-Gualdron, D.A., Camp, J.S., Chung, Y.G., Martin, R.L., Mercado, R., Deem, M.W., Gunter, D., Haranczyk, M.*, et al.* (2015). The materials genome in action: identifying the performance limits for methane storage. Energy Environ Sci *8*, 1190-1199.

Stewart, L., Lu, W., Wei, Z.-W., Ila, D., Padilla, C., and Zhou, H.-C. (2017). A zirconium metal-organic framework with an exceptionally high volumetric surface area. Dalton Trans *46*, 14270-14276.

Tan, J.C., and Cheetham, A.K. (2011). Mechanical properties of hybrid inorganic-organic framework materials: establishing fundamental structure-property relationships. Chem Soc Rev *40*, 1059-1080.

Tan, K., Nijem, N., Canepa, P., Gong, Q., Li, J., Thonhauser, T., and Chabal, Y.J. (2012). Stability and Hydrolyzation of Metal Organic Frameworks with Paddle-Wheel SBUs upon Hydration. Chem Mater *24*, 3153-3167.

Teplensky, M.H., Fantham, M., Li, P., Wang, T.C., Mehta, J.P., Young, L.J., Moghadam, P.Z., Hupp, J.T., Farha, O.K., Kaminski, C.F.*, et al.* (2017). Temperature Treatment of Highly Porous Zirconium-Containing Metal–Organic Frameworks Extends Drug Delivery Release. J Am Chem Soc *139*, 7522-7532.

Thornton, A.W., Simon, C.M., Kim, J., Kwon, O., Deeg, K.S., Konstas, K., Pas, S.J., Hill, M.R., Winkler, D.A., Haranczyk, M.*, et al.* (2017). Materials Genome in Action: Identifying the Performance Limits of Physical Hydrogen Storage. Chem Mater *29*, 2844-2854.

Tian, T., Zeng, Z., Vulpe, D., Casco, M.E., Divitini, G., Midgley, P.A., Silvestre-Albero, J., Tan, J.-C., Moghadam, P.Z., and Fairen-Jimenez, D. (2018). A sol–gel monolithic metal–organic framework with enhanced methane uptake. Nat Mater *17*, 174-179.

Vanduyfhuys, L., Rogge, S.M.J., Wieme, J., Vandenbrande, S., Maurin, G., Waroquier, M., and Van Speybroeck, V. (2018a). Thermodynamic insight into stimuli-responsive behaviour of soft porous crystals. Nat Commun *9*, 204.

Vanduyfhuys, L., Vandenbrande, S., Verstraelen, T., Schmid, R., Waroquier, M., and Van Speybroeck, V. (2015). QuickFF: A program for a quick and easy derivation of force fields for metal-organic frameworks from ab initio input. J Comput Chem *36*, 1015-1027.

Vanduyfhuys, L., Vandenbrande, S., Wieme, J., Waroquier, M., Verstraelen, T., and Van Speybroeck, V. (2018b). Extension of the QuickFF force field protocol for an improved accuracy of structural, vibrational, mechanical and thermal properties of metal–organic frameworks. J Comput Chem *39*, 999-1011.

Verpoort, P.C., MacDonald, P., and Conduit, G.J. (2018). Materials data validation and imputation with an artificial neural network. Comput Mater Sci *147*, 176-185.

Wang, H., Zhu, Q.-L., Zou, R., and Xu, Q. (2017). Metal-Organic Frameworks for Energy Applications. Chem *2*, 52-80.

Willems, T.F., Rycroft, C.H., Kazi, M., Meza, J.C., and Haranczyk, M. (2012). Algorithms and tools for high-throughput geometry-based analysis of crystalline porous materials. Micropor Mesopor Mater *149*, 134-141.

Wilmer, C.E., Leaf, M., Lee, C.Y., Farha, O.K., Hauser, B.G., Hupp, J.T., and Snurr, R.Q. (2012). Large-scale screening of hypothetical metal–organic frameworks. Nat Chem *4*, 83-89.

Wu, H., Yildirim, T., and Zhou, W. (2013). Exceptional Mechanical Stability of Highly Porous Zirconium Metal–Organic Framework UiO-66 and Its Important Implications. The Journal of Physical Chemistry Letters *4*, 925-930.

Xiao, C., and Xie, Y. (2017). The Expanding Energy Prospects of Metal Organic Frameworks. Joule *1*, 25-28.

Zhang, H., Nai, J., Yu, L., and Lou, X.W. (2017). Metal-Organic-Framework-Based Materials as Platforms for Renewable Energy and Environmental Applications. Joule *1*, 77-107.

Zhou, H.C., and Kitagawa, S. (2014). Metal-organic frameworks (MOFs). Chem Soc Rev *43*, 5415-5418.